

**Anomalous bilayer quantum Hall effect**Gurjyot Sethi <sup>1</sup>, D. N. Sheng <sup>2</sup>, and Feng Liu <sup>1</sup><sup>1</sup>*Department of Materials Science & Engineering, University of Utah, Salt Lake City, Utah 84112, USA*<sup>2</sup>*Department of Physics & Astronomy, California State University, Northridge, California 91330, USA* (Received 7 April 2023; revised 6 July 2023; accepted 11 October 2023; published 25 October 2023)

In parallel to the condensed-matter realization of quantum Hall (Chern insulators), quantum spin Hall (topological insulators), and fractional quantum Hall (fractional Chern insulators) effects, we propose that bilayer flat band (FB) lattices with one FB in each layer constitute solid-state analogs of bilayer quantum Hall (BQH) system, leading to anomalous BQH effect without a magnetic field. By exact diagonalization of a bilayer kagome lattice Hamiltonian, as a prototypical example, we demonstrate the stabilization of excitonic condensate Halperin's (1,1,1) state at the total filling  $\nu_T = 1$  of the two FBs. Furthermore, by tuning the interlayer tunneling and distance between the kagome layers at  $\nu_T = 2/3$ , we show phase transitions among Halperin's (3,3,0), spin-singlet (1,1,2), and particle-hole conjugate of Laughlin's  $1/3$  states, as previously observed in conventional BQH systems. Our work opens a new direction in the field of FB physics by demonstrating bilayer FB materials as an attractive avenue for realizing exotic anomalous BQH states including non-Abelian anyons.

DOI: [10.1103/PhysRevB.108.L161112](https://doi.org/10.1103/PhysRevB.108.L161112)

Condensed-matter realization of the quantum Hall effect (QHE), first proposed by Haldane [1], has been one of the most significant scientific breakthroughs that instigated the origin of topological states of matter. Subsequently, topological insulators exhibiting quantum spin Hall effect were proposed by Kane-Mele [2,3] and Bernevig-Hughes-Zhang [4], further fostering the field of topological materials [4,5]. Of particular latest interest is the interplay between topology and electron interaction, inherent to a topological flat band (FB). Two-dimensional (2D) lattices hosting Chern FBs [6–9] have been shown to stabilize the fractional QH (FQH) effect without a magnetic field, manifesting a fractional Chern insulator (FCI) as a condensed matter analog of the FQH effect [10–12]. The anyonic statistics followed by emergent excitations of FQH systems [13–15] make them appealing due to the potential application of non-Abelian anyons in topological quantum computation [16,17].

Beyond single-component FQH, on the other hand, multicomponent FQH effects offer a richer and more exotic quantum phase diagram, with extra degrees of freedom allowing for additional tuning parameters [18–20]. Bilayer quantum Hall (BQH) systems, such as GaAs quantum wells [21–24], are spectacular examples of the multicomponent FQH effect. Either a wide quantum well or a double quantum well can be mapped onto two layers of two-dimensional electron gas separated by a finite distance [Fig. 1(a)] forming the two-component FQH setup, leading to exotic multicomponent quantum Hall plateaus [21–24]. In addition, BQH systems are known to host a plethora of Abelian and non-Abelian FQH phase transitions owing to exceptional tunability of parameters, such as interlayer distance and tunneling strength, which has generated a lot of theoretical and experimental interest [25–30].

In parallel to anomalous QH and FQH effects, the concept of anomalous BQH effect is quite appealing since it could lead to tunable exotic phases, including excitonic superfluid

[31,32], and non-Abelian anyons with two-body interactions at  $\nu_T < 1$  [26,28], while its realization in single-component FCIs requires strong  $n$ -body interaction ( $n > 2$ ) [33–35] or  $\nu_T > 1$  [36,37]. So far, however, the material realization of BQH effect without a magnetic field has remained elusive. Some recent works [38–40] discussed the possibility of stabilizing multicomponent bosonic/fermionic FQH states in a single FB partially filled by spin-up and -down electrons. However, this is extremely hard, if not impossible, to do experimentally; also, the tunability of intercomponent interaction and tunneling strength, an essential element of BQH systems, is entirely lacking. It is also worth noting that some earlier works [41–43] illustrated the stabilization of multicomponent FQH states in higher Chern number FBs, although still lacking in tunability and experimental feasibility.

In this Letter, we propose a *direct solid-state analog* of the BQH effect, to open the door for its materials realization by exploiting a two-layer FB system whose layer index of the two separate layers is easily accessible in experiments, in contrast to spin index within the same band. We use a bilayer kagome lattice [Fig. 1(b)] as a prototypical example, which is one of the most widely studied 2D lattices and material systems hosting topological FBs [7,44–47]. Excitingly, a recent experiment observed the topological FB in a *monolayer* breathing-kagome lattice [48], and bilayer-kagome-lattice materials have also been experimentally synthesized as candidates to host quantum spin liquids [49,50]. In addition, topological FBs are proposed in multilayer heterostructures [51,52], as well as in metal-organic frameworks [53–56].

Importantly, using layer degree of freedom instead of spin, the intercomponent interactions and tunneling strength become highly tunable. The individual FB layers can be separated by a tunneling barrier [57] [Fig. 1(c)]; then one may access different phase regions by systematically tuning the tunneling barrier materials and interlayer distance,

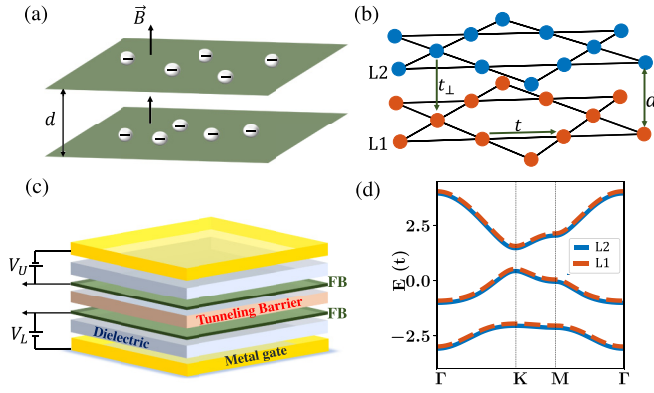


FIG. 1. (a) Schematic of BQH setup containing two layers of 2D electron gas separated by a distance  $d$  and a tunneling barrier. (b) Schematic of bilayer kagome lattice with blue and orange colors indicating atoms in layers L1 and L2 respectively. (c) Schematic of possible device configuration that can be used to realize anomalous BQH effect.  $V_U(L)$  represent gate voltages for upper (lower) layer. FB material is indicated by a green layer with a tunneling barrier in between. (d) Single-particle band structure of bilayer kagome lattice at  $\lambda = 0.3t$  and  $t_{\perp} = 0$ . The two FBs belonging to individual layers are depicted in blue and orange color respectively.

and at the weak tunneling limit with a high barrier one can change the distance and hence interlayer Coulomb interaction independently [23,58]. This is very crucial for realizing different exotic Abelian/non-Abelian phase transitions hosted in anomalous BQH systems as we propose, which directly mimic the conventional BQH systems fabricated using double quantum wells [23]. Here, using the exact diagonalization (ED) method, we demonstrate characteristic signatures of anomalous BQH states in a bilayer kagome lattice. We have calculated topological degeneracy of the ground-state manifold on a torus, a nontrivial Chern matrix, and excitonic off-diagonal long-range order, to prove the stabilization of excitonic condensate states at total filling  $\nu_T = 1$  of two FBs, and further illustrate the potential of this lattice in stabilizing exotic tunable anomalous BQH states at  $\nu_T = 2/3$ . We use a nearest-neighbor (NN) tight-binding model of a bilayer kagome lattice [Fig. 1(b)] with spin-orbit coupling (SOC) that conserves the out-of-plane spin-component [44], leading to the kinetic part of the total Hamiltonian in the absence of interlayer tunneling,

$$H_{\text{kin}} = \sum_{\sigma} \left[ -t \sum_{\langle i,j \rangle \alpha} c_{i\sigma\alpha}^{\dagger} c_{j\sigma\alpha} + i\lambda \sum_{\langle i,j \rangle \alpha\beta} \frac{2}{\sqrt{3}} (\mathbf{r}_{ki} \times \mathbf{r}_{kj}) \cdot \boldsymbol{\tau}_{\alpha\beta} c_{i\sigma\alpha}^{\dagger} c_{j\sigma\beta} \right] \quad (1)$$

where  $t$  is the NN hopping integral,  $\lambda$  represents SOC strength,  $\mathbf{r}_{ki}$  and  $\mathbf{r}_{kj}$  are the two NN unit vectors pointing from atomic site  $k$  to  $i$  and  $j$  respectively with  $i, j$ , and  $k$  forming a triangle in the kagome lattice (see Fig. S1 in the Supplemental Material (SM) [59]),  $\alpha(\beta)$  are spin indices,  $\boldsymbol{\tau} = (\tau_x, \tau_y, \tau_z)$  with  $\tau_i$  being the  $i$ th Pauli's matrix, and  $\sigma(\sigma')$  represents each layer of the bilayer lattice. Electron interactions are described

by an extended Hubbard model including NN intralayer ( $V$ ) and direct interlayer ( $V_{\perp}$ ) interactions.  $V_{\perp}$  depends on the interlayer distance  $d$  as shown in Fig. 1(b), and can be varied easily, rendering the tunability of inter-component interactions. We also include tunneling between the layers ( $t_{\perp}$ ) in the interaction part of the Hamiltonian, which is given as

$$H_{\text{int}} = \sum_{\sigma, \sigma'} \left[ V \sum_{\langle r, r' \rangle_{\text{intra}}} n_{r\sigma} n_{r'\sigma'} + V_{\perp} \sum_r n_{r\sigma} n_{r\sigma'} + t_{\perp} \sum_r c_{r\sigma}^{\dagger} c_{r\sigma'} \right] \quad (2)$$

where  $n_{r\sigma} = c_{r\sigma}^{\dagger} c_{r\sigma}$  is the electron density operator. The spin indices are suppressed. Throughout this work we set  $V = 2t$ , which is smaller than the single-particle gap separating the FBs [Fig. 1(b)], while a distance dependence of  $V_{\perp} = 1.5t/d$  is assumed. Note that  $d$  (hence  $V_{\perp}$ ) and  $t_{\perp}$  can be systematically varied in general and independently in a bilayer FB setup at the weak tunneling limit, as mentioned above [23,58].

Single-particle band structure is shown in Fig. 1(d). With  $t_{\perp} = 0$ , the two layer-indexed FBs have the same Chern numbers, which exactly match the two Landau levels in each layer of a conventional BQH system. We use a slightly high SOC ( $\lambda = 0.3t$ ) to isolate the bottom FBs from other bands. This procedure is widely used in realizing FCI where a high flatness ratio of FB is desirable [44]. It is worth mentioning that such conditional parameters can be realized using Floquet band engineering in real materials [47,60]. To study the effect of interactions, we exactly diagonalize the full Hamiltonian ( $H = H_{\text{kin}} + H_{\text{int}}$ ) in reciprocal space with interactions projected to the two FBs of a finite lattice containing a total number of  $N_s = 6 \times N_x \times N_y$  sites. The total filling factor is given by  $\nu_T = N_e / (N_x \times N_y)$ , where  $N_e$  is the number of electrons in the system. Under periodic boundary condition, we implement translational symmetry and diagonalize the Hamiltonian in each momentum sector  $q = (2\pi k_x / N_x, 2\pi k_y / N_y)$  with  $k_x$  and  $k_y$  being the integers, labeled as  $(k_x, k_y)$ . One can also assign a pseudospin notation to each FB and define  $S_z = (N_{\uparrow} - N_{\downarrow})/2$ , where  $N_{\uparrow(\downarrow)}$  is the number of electrons in FB belonging to the upper (lower) layer.  $S_z$  is a good quantum number when  $t_{\perp} = 0$ . Detailed methodology of ED for multiple bands can be found in earlier work [61] (also see SM Sec. I [59]).

First, we study the  $\nu_T = 1$  case. Multicomponent FQH systems are described by Halperin's  $(m, m, n)$  wave functions [18]. In the following, we only use integers  $(m, m, n)$  to refer to these states. In a BQH setup with negligible  $t_{\perp}$ , the  $\nu_T = 1$  plateau is described by  $(1, 1, 1)$  state featuring a nondegenerate ground state on two tori [40]. In Fig. 2(a) we plot the energy spectra for  $S_z = 0$ , or the case of balanced layers with  $N_{\uparrow} = N_{\downarrow}$ , at a finite  $d = 0.3a$  and negligible  $t_{\perp}$ . There is clearly the presence of a nondegenerate ground state separated from excited states in two systems of different sizes, which are shown to confirm the convergence of our results. For all subsequent calculations the system size of  $4 \times 3$  is used. The  $(1, 1, 1)$  state on two tori should belong to the total momentum sector  $(\sum_{i=1}^N k_x^i, \sum_{i=1}^N k_y^i)$ , where  $N = N_x \times N_y$ , implying that all the reciprocal points are occupied; for the  $4 \times 3$  system, it

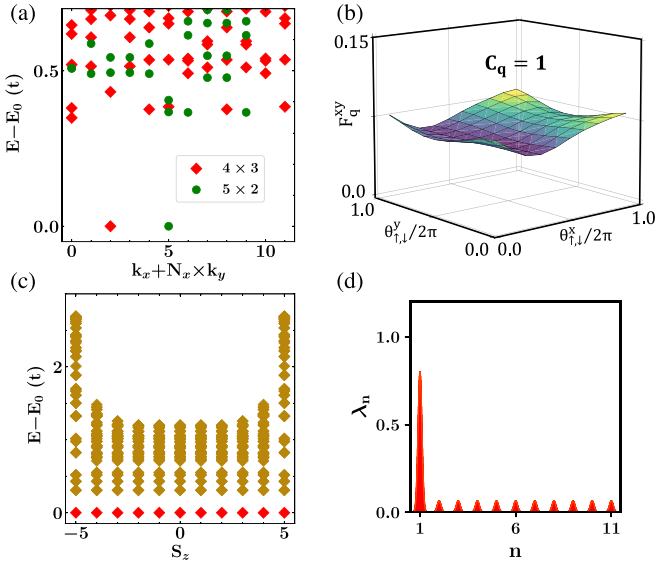


FIG. 2. (a) Momentum-resolved spectra of  $H$  at  $d = 0.3a$ ,  $t_{\perp} = 0$ , and  $S_z = 0$  for two system sizes,  $N_s = 6 \times 5 \times 2$  and  $N_s = 6 \times 4 \times 3$  denoted by green circles and red diamonds respectively. (b) Berry curvature for total charge Chern number indicated by  $C_q$ . (c) Energy spectra of  $H$  at  $d \rightarrow 0$  and  $t_{\perp} = 0$  with varying  $S_z$  for  $N_s = 6 \times 4 \times 3$ . Red (yellow) diamonds denote the ground (excited) states. (d) Eigenvalues of  $\rho^{(2)}$  for (b) plotted in descending order.

is the (2,0) sector, as shown in Fig. 2(a), implying a nontrivial topology of the ground state with a binding of particle-hole between two layers. Beyond the energy spectra, we extract the Chern number matrix  $C = \begin{bmatrix} C_{\uparrow\uparrow} & C_{\uparrow\downarrow} \\ C_{\downarrow\uparrow} & C_{\downarrow\downarrow} \end{bmatrix}$  for the two-component FQH system, which contains information for quantized Hall conductance [27,38–40]. For Abelian multicomponent FQH states, the diagonal and off-diagonal elements of  $C$  are related to intra- and intercomponent Hall transports respectively. Each component of  $C$  is defined under twisted boundary conditions with  $\theta_{\uparrow(\downarrow)}^{x(y)}$  being the twist angle in layer  $\uparrow(\downarrow)$  in the  $x$  ( $y$ ) direction [38–40,59,62]. With  $\theta_{\uparrow}^x = \theta_{\downarrow}^x = \theta^x$  and  $\theta_{\uparrow}^y = \theta_{\downarrow}^y = \theta^y$ , charge Hall conductance is related to  $C_q = \sum_{\sigma,\sigma'} C_{\sigma,\sigma'}$ . For the single nondegenerate ground state at  $\nu_T = 1$ , we numerically calculate Berry curvatures on an  $11 \times 11$  mesh in the phase space and obtain a topological invariant  $C_q = 1$  with a well-defined smooth Berry curvature as plotted in Fig. 2(b), further confirming the nontrivial topology of the (1,1,1) state.

A fundamental global property of Halperin’s (1,1,1) ground state at  $\nu_T = 1$  is the binding of electrons in one layer to the empty states (holes) in the other layer. Such interlayer excitons form a coherent superfluid which has been observed in counterflow transport measurements. In fact, bilayer quantum Hall systems are the only physical systems where this exotic transport property of excitonic superfluid has been observed [31,32,57], albeit under a strong magnetic field. Next, we show excitonic properties of the ground state in a bilayer kagome lattice at  $\nu_T = 1$  without a magnetic field. In Fig. 2(c) we show the energy spectra of  $H$  for  $\nu_T = 1$  with negligible  $d$  and  $t_{\perp}$  at multiple  $S_z$ , which determines the relative number of electrons in each FB. The degeneracy of states with varying  $S_z$  indicates that there is no energy cost for electrons to

tunnel in between the two layers, a signature of spontaneous symmetry breaking, also known as the “which layer” uncertainty [32]. This leads to a huge interlayer tunneling current at zero energy as observed in double quantum well BQH experiments [31]. At a finite  $d$ , the state with  $S_z = 0$  becomes energetically stable due to anisotropy in interactions (see SM Sec. II [59]).

We further illustrate excitonic coherence order by calculating eigenvalues of the excitonic reduced two-body density matrix [61],  $\rho^{(2)}(k, k'; \bar{k}, \bar{k}') = \langle \Psi | \psi_2^{\dagger}(k) \psi_1(k') \psi_1^{\dagger}(\bar{k}') \psi_2(\bar{k}) | \Psi \rangle$ , where  $\psi_{1(2)}^{\dagger}(k)$  creates an electron in the FB belonging to layer 1 (2) at reciprocal lattice point  $k$ , and  $|\Psi\rangle$  is the many-body ground-state wave-function. The eigenvalues of the two-body density matrix are the occupations of bosonic natural orbitals. Hence, the presence of one large eigenvalue signifies Bose-Einstein condensation. In Fig 2(d), we plot the normalized eigenvalues ( $\lambda_n$ ), i.e., eigenvalues divided by the total number of excitons in the system (for a system size  $4 \times 3$ , it is 6) in descending order, so that the presence of one large, normalized eigenvalue of order 1 concretely shows the presence of excitonic superfluid. At  $d \sim 0.3a$ , there is indeed one large eigenvalue  $\sim 0.8$ , implying that 80% of excitons are in the same natural orbital. We note that if the interlayer distance is reduced further, the condensation factor is enhanced as expected (Fig. S2 in SM [59]). This concretely shows the presence of a symmetry-broken condensate order parameter pointing to the possible experimental observation of excitonic superfluid in counterflow transport measurements without a magnetic field in bilayer FB lattices. Next, we focus on filling factor  $\nu_T = 2/3$ , in order to illustrate the tunability of anomalous BQH states as realized in the bilayer kagome system. At  $\nu_T = 2/3$  and a relatively large  $d = 2.25a$  between the two layers, we plot the energy spectrum for balanced layers ( $S_z = 0$ ), as depicted in Fig. 3(a). The individual layers are decoupled when  $d$  is large and should stabilize the (3,3,0) state [28], which is simply the bilayer Laughlin’s state. We first use topological degeneracy of the ground-state manifold on a torus to identify the nontrivial character of this state [63–65]. Intercomponent correlations in the  $(m, m, n)$  state, in general, can be studied using the  $K$  matrix,  $K = \begin{bmatrix} m & n \\ n & m \end{bmatrix}$ , as formulated within the field theory framework [66,67]. Topological degeneracy of the ground state for a system with  $\nu_T = p/q$  on a torus is given by the determinant of the  $K$  matrix,  $\det K = qN'$ , where  $N'$  is an integer describing different translations of the individual center of mass (COM) of a component, while  $q$  determines the overall COM degeneracy. In the case of the (3,3,0) state at  $\nu_T = 2/3$ , and a  $4 \times 3$  system size, the three degenerate states corresponding to  $N' = 3$  should lie at (0,0) [61]. Taking COM degeneracy into account there should be an additional threefold degeneracy for each of these states, as depicted in Fig. 3(a).

To further illustrate this state to be topologically ordered, we calculate the  $C$  matrix (which should be  $= K^{-1}$  [27]) for the nine quasidegenerate ground states of the (3,3,0) state. For the three states at (0,0), we found that the intracomponent Berry curvature is well defined and smooth [Fig. 3(b)], from which we obtain a  $C$  matrix element,  $\sum_{i=1}^3 C_{\uparrow\uparrow} = 1$ , while the off-diagonal element of the  $C$  matrix vanishes ( $\sum_{i=1}^3 C_{\uparrow\downarrow} = 0$ ). Similarly, for all the nine

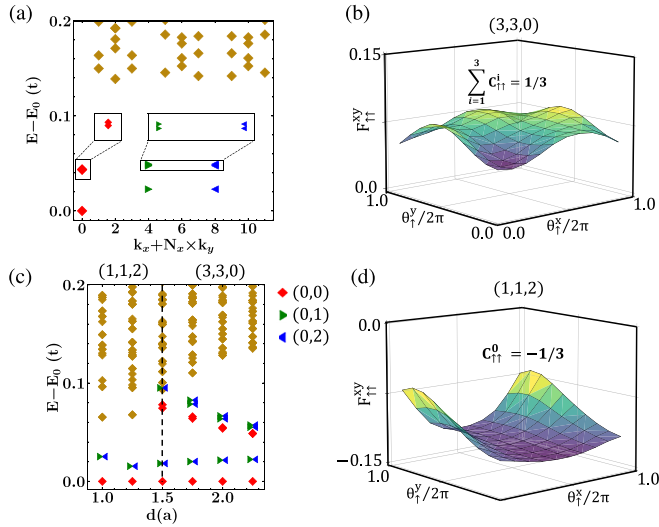


FIG. 3. (a) Energy spectra of  $H$  at  $d = 2.25a$  and  $t_{\perp} = 0$  for  $N_s = 6 \times 4 \times 3$  system size. Red diamonds (0,0) and blue (0,1) and green (0,2) triangles denote the ninefold degenerate ground-state manifold while yellow denotes the excited states. The inset shows the zoomed-in view of ground-state manifold. (b) Total intracomponent Berry curvature ( $C_{\uparrow\uparrow}^0$ ) of the three quasidegenerate states at (0,0) for the system in (a). (c)  $d$ -driven phase transition from the (1,1,2) state to the (3,3,0) state. (d) Intracomponent Berry curvature ( $C_{\uparrow\uparrow}^0$ ) for the single state at (0,0) of the threefold degenerate ground-state manifold of (1,1,2) calculated at  $d = 1.0a$ .

states in momentum sectors (0,0), (0,1), and (0,2), we obtain  $\sum_{i=1}^9 C_{\uparrow\uparrow} = 3$  and  $\sum_{i=1}^9 C_{\downarrow\downarrow} = 0$ . The other two elements are related to these two by symmetry  $c_{\uparrow} \rightarrow c_{\downarrow}$ . This finally gives

$$C = \begin{bmatrix} C_{\uparrow\uparrow} & C_{\uparrow\downarrow} \\ C_{\downarrow\uparrow} & C_{\downarrow\downarrow} \end{bmatrix} = \frac{1}{9} \begin{bmatrix} 3 & 0 \\ 0 & 3 \end{bmatrix}, \quad (3)$$

which is the inverse of the  $K$  matrix for the (3,3,0) state, proving the topological characteristic of this state. In addition, we calculate the spectral flow of these nine states under flux insertion, confirming fractional charge Hall conductance (Figs. S3(a) and S3(b) [59]).

Next, we show a  $d$ -driven transition from the spin-singlet (1,1,2) state at small  $d$  to the (3,3,0) state at large  $d$  in Fig. 3(c). When  $d$  is small, the  $\nu_T = 2/3$  anomalous BQH resembles the usual  $\nu_T = 2/3$  FQH state with spin; i.e., for small  $d$  the pseudospin can be directly mapped onto electronic spin, which stabilizes the (1,1,2) state with threefold degeneracy on a torus [27]. In Fig. 3(c) we show a transition from the three- to ninefold degenerate ground state, as  $d$  increases, with gap closing at  $d = 1.5a$ . The latter ( $d > 1.5a$ ) is identified as the (3,3,0) state having the  $C$  matrix as shown in Eq. (3); the former ( $d < 1.5a$ ) is characterized with  $C = \frac{1}{3} \begin{bmatrix} -1 & 2 \\ 2 & -1 \end{bmatrix}$ , as expected for the (1,1,2) state, numerically calculated from the inter- and intracomponent Berry curvature [Fig. 3(d)]. We note that the energy spread of the ground-state manifold in Fig. 3(c) is comparable to the many-body gap near the phase transition point. This is not an artifact of the finite-size effect but signifies a topological phase transition involving gap closing and reopening with different numbers of states in

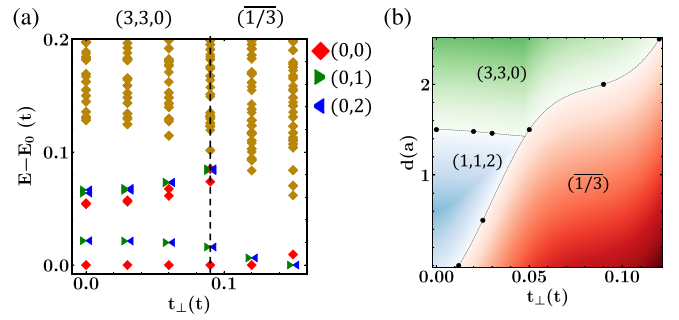


FIG. 4. (a)  $t_{\perp}$ -driven phase transition at  $\nu_T = 2/3$ ,  $d = 2.0a$ ,  $S_z = 0$  for  $N_s = 6 \times 4 \times 3$  system size. (b) Phase diagram for a bilayer kagome lattice at  $\nu_T = 2/3$  in the phase space of  $d$  and  $t_{\perp}$  between the two kagome layers.

the ground-state manifold on two sides of the transition point. There is also a possibility of  $t_{\perp}$ -driven transition at  $\nu_T = 2/3$  [28]. In Fig. 4(a) we show a transition from the (3,3,0) state to the particle-hole conjugate of Laughlin's  $1/3$  state ( $\overline{1/3}$ ) at  $d = 2.0a$ . At weak  $t_{\perp}$ , the (3,3,0) state is identified using the  $C$  matrix as described earlier. At strong  $t_{\perp}$ , the bilayer effectively behaves as a single layer due to strong correlations and stabilizes the  $\overline{1/3}$  state with threefold COM degeneracy at (0,0), (0,1), and (0,2), which is also seen in Fig. 4(a), similarly to the BQH system [32]. Hence, in the phase space of  $t_{\perp}$  and  $d$ , we identify three phases: (3,3,0) state at large  $d$  and weak  $t_{\perp}$ ; (1,1,2) state at small  $d$  and weak  $t_{\perp}$ ;  $\overline{1/3}$  state at small  $d$  and strong  $t_{\perp}$ , as shown by the phase diagram in Fig. 4(b). The phase transition boundary from the threefold degenerate (1,1,2) to the  $\overline{1/3}$  state is obtained using gap-closing and -reopening points (Fig. S3(c) [59]). This phase diagram for the bilayer FB lattice is in excellent agreement with the one found in a conventional BQH system [28].

In addition to the exceptional tunability of bilayer FB lattices, an important aspect of realizing the exotic anomalous BQH states in such systems is their experimental feasibility. Recently, FCI was experimentally identified in twisted bilayer graphene over a hexagonal boron nitride substrate under a weak magnetic field [68] and in a twisted bilayer transition metal dichalcogenide without a magnetic field [69]. A promising way to realize anomalous BQH states is to construct two such bilayers separated by a tunneling barrier (Fig. 1(b)). Moreover, Floquet engineering of isolated FBs has been shown as a promising route towards realizing FCIs in 2D materials, for example, graphene [60], and a metal-organic 2D monolayer with kagome bands [47]. This approach can be generalized to bilayers of such FB materials. One possibility is using Floquet engineering to isolate two FBs of bilayers such as superatomic graphene lattice, whose single-layer structure has already been experimentally synthesized using molecular building blocks of triangulene [70] (also see SM Sec. VI [59]). In addition, the striking tunability of anomalous BQH states, as illustrated here for a bilayer kagome lattice, could also lead to material realization of non-Abelian anyonic states without a magnetic field. We observe some preliminary signatures of such exotic states (SM Sec. V [59]) whose further investigation has been left for future work.

We thank Y. S. Wu for helpful discussions. G.S. and F.L. acknowledge support from U.S. Department of Energy (DOE)–Basic Energy Sciences under Grant No. DE-FG02-04ER46148. D.N.S. acknowledges support by the

U.S. DOE–Basic Energy Sciences under Grant No. DE-FG02-334 06ER46305 for studying topological states. All calculations were done on the CHPC at the University of Utah.

- 
- [1] F. D. M. Haldane, Model for a quantum Hall effect without Landau levels: Condensed-matter realization of the “parity anomaly”, *Phys. Rev. Lett.* **61**, 2015 (1988).
- [2] C. L. Kane and E. J. Mele, Quantum spin Hall effect in graphene, *Phys. Rev. Lett.* **95**, 226801 (2005).
- [3] C. L. Kane and E. J. Mele,  $Z_2$  topological order and the quantum spin Hall effect, *Phys. Rev. Lett.* **95**, 146802 (2005).
- [4] B. A. Bernevig, T. L. Hughes, and S.-C. Zhang, Quantum spin Hall effect and topological phase transition in HgTe quantum wells, *Science* **314**, 1757 (2006).
- [5] C.-Z. Chang, J. Zhang, X. Feng, J. Shen, Z. Zhang, M. Guo, K. Li, Y. Ou, P. Wei, L.-L. Wang *et al.*, Experimental observation of the quantum anomalous Hall effect in a magnetic topological insulator, *Science* **340**, 167 (2013).
- [6] E. J. Bergholtz and Z. Liu, Topological flat band models and fractional Chern insulators, *Int. J. Mod. Phys. B* **27**, 1330017 (2013).
- [7] Z. Liu, F. Liu, and Y.-S. Wu, Exotic electronic states in the world of flat bands: From theory to material, *Chin. Phys. B* **23**, 077308 (2014).
- [8] J. Wang, J. Cano, A. J. Millis, Z. Liu, and B. Yang, Exact Landau level description of geometry and interaction in a flatband, *Phys. Rev. Lett.* **127**, 246403 (2021).
- [9] B. Estienne, N. Regnault, and V. Crépel, Ideal Chern bands are Landau levels in curved space, *Phys. Rev. Res.* **5**, L032048 (2023).
- [10] D. Sheng, Z.-C. Gu, K. Sun, and L. Sheng, Fractional quantum Hall effect in the absence of Landau levels, *Nat. Commun.* **2**, 389 (2011).
- [11] N. Regnault and B. A. Bernevig, Fractional Chern insulator, *Phys. Rev. X* **1**, 021014 (2011).
- [12] P. J. Ledwith, A. Vishwanath, and D. E. Parker, Vortexability: A unifying criterion for ideal fractional Chern insulators, [arXiv:2209.15023](https://arxiv.org/abs/2209.15023).
- [13] F. D. M. Haldane, Fractional quantization of the Hall effect: A hierarchy of incompressible quantum fluid states, *Phys. Rev. Lett.* **51**, 605 (1983).
- [14] B. I. Halperin, Statistics of quasiparticles and the hierarchy of fractional quantized Hall states, *Phys. Rev. Lett.* **52**, 1583 (1984).
- [15] D. Arovas, J. R. Schrieffer, and F. Wilczek, Fractional statistics and the quantum Hall effect, *Phys. Rev. Lett.* **53**, 722 (1984).
- [16] G. Moore and N. Read, Nonabelions in the fractional quantum Hall effect, *Nucl. Phys. B* **360**, 362 (1991).
- [17] C. Nayak, S. H. Simon, A. Stern, M. Freedman, and S. D. Sarma, Non-Abelian anyons and topological quantum computation, *Rev. Mod. Phys.* **80**, 1083 (2008).
- [18] B. I. Halperin, Theory of the quantized Hall conductance, *Helv. Phys. Acta* **56**, 75 (1983).
- [19] X.-G. Wen, Continuous topological phase transitions between clean quantum Hall states, *Phys. Rev. Lett.* **84**, 3950 (2000).
- [20] M. Barkeshli and X.-G. Wen, Bilayer quantum Hall phase transitions and the orbifold non-Abelian fractional quantum Hall states, *Phys. Rev. B* **84**, 115121 (2011).
- [21] Y. W. Suen, L. W. Engel, M. B. Santos, M. Shayegan, and D. C. Tsui, Observation of a  $\nu = 1/2$  fractional quantum Hall state in a double-layer electron system, *Phys. Rev. Lett.* **68**, 1379 (1992).
- [22] J. P. Eisenstein, G. S. Boebinger, L. N. Pfeiffer, K. W. West, and S. He, New fractional quantum Hall state in double-layer two-dimensional electron systems, *Phys. Rev. Lett.* **68**, 1383 (1992).
- [23] Y. W. Suen, H. C. Manoharan, X. Ying, M. B. Santos, and M. Shayegan, Origin of the  $\nu = 1/2$  fractional quantum Hall state in wide single quantum wells, *Phys. Rev. Lett.* **72**, 3405 (1994).
- [24] J. Shabani, Y. Liu, M. Shayegan, L. N. Pfeiffer, K. W. West, and K. W. Baldwin, Phase diagrams for the stability of the  $\nu = 1/2$  fractional quantum Hall effect in electron systems confined to symmetric, wide GaAs quantum wells, *Phys. Rev. B* **88**, 245413 (2013).
- [25] D. N. Sheng, L. Balents, and Z. Wang, Phase diagram for quantum Hall bilayers at  $\nu = 1$ , *Phys. Rev. Lett.* **91**, 116802 (2003).
- [26] W. Zhu, Z. Liu, F. D. M. Haldane, and D. N. Sheng, Fractional quantum Hall bilayers at half filling: Tunneling-driven non-Abelian phase, *Phys. Rev. B* **94**, 245147 (2016).
- [27] I. A. MacDonald and F. D. M. Haldane, Topological phase transition in the  $\nu = 2/3$  quantum Hall effect, *Phys. Rev. B* **53**, 15845 (1996).
- [28] S. Geraedts, M. P. Zaletel, Z. Papić, and R. S. K. Mong, Competing Abelian and non-Abelian topological orders in  $\nu = 1/3 + 1/3$  quantum Hall bilayers, *Phys. Rev. B* **91**, 205139 (2015).
- [29] V. Crépel, B. Estienne, and N. Regnault, Variational ansatz for an Abelian to non-Abelian topological phase transition in  $\nu = 1/2 + 1/2$  bilayers, *Phys. Rev. Lett.* **123**, 126804 (2019).
- [30] Q. Hu, T. Neupert, and G. Wagner, Single-parameter variational wavefunctions for quantum Hall bilayers, [arXiv:2303.12825](https://arxiv.org/abs/2303.12825).
- [31] J. Eisenstein and A. MacDonald, Bose–Einstein condensation of excitons in bilayer electron systems, *Nature (London)* **432**, 691 (2004).
- [32] J. Eisenstein, Exciton condensation in bilayer quantum Hall systems, *Annu. Rev. Condens. Matter Phys.* **5**, 159 (2014).
- [33] Y.-F. Wang, H. Yao, Z.-C. Gu, C.-D. Gong, and D. N. Sheng, Non-Abelian quantum Hall effect in topological flat bands, *Phys. Rev. Lett.* **108**, 126805 (2012).
- [34] Y.-L. Wu, B. A. Bernevig, and N. Regnault, Zoology of fractional Chern insulators, *Phys. Rev. B* **85**, 075116 (2012).
- [35] M. Greiter, X.-G. Wen, and F. Wilczek, Paired Hall state at half filling, *Phys. Rev. Lett.* **66**, 3205 (1991).
- [36] R. Willett, J. P. Eisenstein, H. L. Störmer, D. C. Tsui, A. C. Gossard, and J. H. English, Observation of an even-denominator quantum number in the fractional quantum Hall effect, *Phys. Rev. Lett.* **59**, 1776 (1987).
- [37] K. Pakrouski, M. R. Peterson, T. Jolicoeur, V. W. Scarola, C. Nayak, and M. Troyer, Phase diagram of the  $\nu = 5/2$

- fractional quantum Hall effect: Effects of Landau-level mixing and nonzero width, *Phys. Rev. X* **5**, 021004 (2015).
- [38] T.-S. Zeng, W. Zhu, and D. N. Sheng, Two-component quantum Hall effects in topological flat bands, *Phys. Rev. B* **95**, 125134 (2017).
- [39] T.-S. Zeng and W. Zhu, Chern-number matrix of the non-Abelian spin-singlet fractional quantum Hall effect, *Phys. Rev. B* **105**, 125128 (2022).
- [40] T.-S. Zeng, D. N. Sheng, and W. Zhu, Quantum Hall effects of exciton condensate in topological flat bands, *Phys. Rev. B* **101**, 195310 (2020).
- [41] Y.-F. Wang, H. Yao, C.-D. Gong, and D. N. Sheng, Fractional quantum Hall effect in topological flat bands with Chern number two, *Phys. Rev. B* **86**, 201101(R) (2012).
- [42] Z. Liu, E. J. Bergholtz, H. Fan, and A. M. Läuchli, Fractional Chern insulators in topological flat bands with higher Chern number, *Phys. Rev. Lett.* **109**, 186805 (2012).
- [43] M. Trescher and E. J. Bergholtz, Flat bands with higher Chern number in pyrochlore slabs, *Phys. Rev. B* **86**, 241111(R) (2012).
- [44] E. Tang, J.-W. Mei, and X.-G. Wen, High-temperature fractional quantum Hall states, *Phys. Rev. Lett.* **106**, 236802 (2011).
- [45] Y. Zhou, G. Sethi, H. Liu, Z. Wang, and F. Liu, Excited quantum anomalous and spin Hall effect: Dissociation of flat-bands-enabled excitonic insulator state, *Nanotechnology* **33**, 415001 (2022).
- [46] G. Sethi, Y. Zhou, L. Zhu, L. Yang, and F. Liu, Flat-band-enabled triplet excitonic insulator in a diatomic kagome lattice, *Phys. Rev. Lett.* **126**, 196403 (2021).
- [47] H. Liu, G. Sethi, D. N. Sheng, Y. Zhou, J.-T. Sun, S. Meng, and F. Liu, High-temperature fractional quantum Hall state in the Floquet kagome flat band, *Phys. Rev. B* **105**, L161108 (2022).
- [48] M. Pan, X. Zhang, Y. Zhou, P. Wang, Q. Bian, H. Liu, X. Wang, X. Li, A. Chen, X. Lei *et al.*, Growth of mesoscale ordered two-dimensional hydrogen-bond organic framework with the observation of flat band, *Phys. Rev. Lett.* **130**, 036203 (2023).
- [49] J. M. Ni, Q. Y. Liu, Y. J. Yu, E. J. Cheng, Y. Y. Huang, Z. Y. Liu, X. J. Wang, Y. Sui, and S. Y. Li, Ultralow-temperature heat transport in the quantum spin liquid candidate  $\text{Ca}_{10}\text{Cr}_7\text{O}_{28}$  with a bilayer kagome lattice, *Phys. Rev. B* **97**, 104413 (2018).
- [50] A. Balodhi and Y. Singh, Synthesis and pressure and field-dependent magnetic properties of the kagome-bilayer spin liquid  $\text{Ca}_{10}\text{Cr}_7\text{O}_{28}$ , *Phys. Rev. Mater.* **1**, 024407 (2017).
- [51] L. Balents, C. R. Dean, D. K. Efetov, and A. F. Young, Superconductivity and strong correlations in moiré flat bands, *Nat. Phys.* **16**, 725 (2020).
- [52] Y.-H. Zhang, D. Mao, Y. Cao, P. Jarillo-Herrero, and T. Senthil, Nearly flat Chern bands in moiré superlattices, *Phys. Rev. B* **99**, 075127 (2019).
- [53] T. Kambe, R. Sakamoto, K. Hoshiko, K. Takada, M. Miyachi, J.-H. Ryu, S. Sasaki, J. Kim, K. Nakazato, M. Takata *et al.*,  $\pi$ -conjugated nickel Bis(dithiolene) complex nanosheet, *J. Am. Chem. Soc.* **135**, 2462 (2013).
- [54] W. Jiang, X. Ni, and F. Liu, Exotic topological bands and quantum states in metal-organic and covalent-organic frameworks, *Acc. Chem. Res.* **54**, 416 (2021).
- [55] X. Ni, H. Li, F. Liu, and J.-L. Brédas, Engineering of flat bands and dirac bands in two-dimensional covalent organic frameworks (COFs): Relationships among molecular orbital symmetry, lattice symmetry, and electronic-structure characteristics, *Mater. Horizons* **9**, 88 (2022).
- [56] Z. Liu, Z.-F. Wang, J.-W. Mei, Y.-S. Wu, and F. Liu, Flat Chern band in a two-dimensional organometallic framework, *Phys. Rev. Lett.* **110**, 106804 (2013).
- [57] J. Li, T. Taniguchi, K. Watanabe, J. Hone, and C. Dean, Excitonic superfluid phase in double bilayer graphene, *Nat. Phys.* **13**, 751 (2017).
- [58] N. Kumada, D. Terasawa, Y. Shimoda, H. Azuhata, A. Sawada, Z. F. Ezawa, K. Muraki, T. Saku, and Y. Hirayama, Phase diagram of interacting composite fermions in the bilayer  $\nu = 2/3$  quantum Hall effect, *Phys. Rev. Lett.* **89**, 116802 (2002).
- [59] See Supplemental Material at <http://link.aps.org/supplemental/10.1103/PhysRevB.108.L161112> for discussion on computational methods, spectral flow analysis, preliminary signature of possible non-Abelian state at  $\nu_T = 2/3$ , and material realization of the anomalous BQH effect, which includes Refs. [71–73].
- [60] A. G. Grushin, Á. Gómez-León, and T. Neupert, Floquet fractional Chern insulators, *Phys. Rev. Lett.* **112**, 156801 (2014).
- [61] G. Sethi, M. Cuma, and F. Liu, Excitonic condensate in flat valence and conduction bands of opposite chirality, *Phys. Rev. Lett.* **130**, 186401 (2023).
- [62] Q. Niu, D. J. Thouless, and Y.-S. Wu, Quantized Hall conductance as a topological invariant, *Phys. Rev. B* **31**, 3372 (1985).
- [63] R. Tao and Y.-S. Wu, Gauge invariance and fractional quantum Hall effect, *Phys. Rev. B* **30**, 1097 (1984).
- [64] F. D. M. Haldane, Many-particle translational symmetries of two-dimensional electrons at rational Landau-level filling, *Phys. Rev. Lett.* **55**, 2095 (1985).
- [65] I. A. McDonald, Degeneracy of multicomponent quantum Hall states satisfying periodic boundary conditions, *Phys. Rev. B* **51**, 10851 (1995).
- [66] X.-G. Wen and A. Zee, Classification of Abelian quantum Hall states and matrix formulation of topological fluids, *Phys. Rev. B* **46**, 2290 (1992).
- [67] B. Blok and X.-G. Wen, Effective theories of the fractional quantum Hall effect at generic filling fractions, *Phys. Rev. B* **42**, 8133 (1990).
- [68] Y. Xie, A. T. Pierce, J. M. Park, D. E. Parker, E. Khalaf, P. Ledwith, Y. Cao, S. H. Lee, S. Chen, P. R. Forrester *et al.*, Fractional Chern insulators in magic-angle twisted bilayer graphene, *Nature (London)* **600**, 439 (2021).
- [69] J. Cai, E. Anderson, C. Wang, X. Zhang, X. Liu, W. Holtzmann, Y. Zhang, F. Fan, T. Taniguchi, K. Watanabe *et al.*, Signatures of fractional quantum anomalous Hall states in twisted  $\text{MoTe}_2$ , *Nature* **622**, 63 (2023).
- [70] A. Delgado, C. Dusold, J. Jiang, A. Cronin, S. G. Louie, and F. R. Fischer, Evidence for excitonic insulator ground state in triangulene kagome lattice, [arXiv:2301.06171](https://arxiv.org/abs/2301.06171).
- [71] A. W. Sandvik, Computational studies of quantum spin systems, in *Lectures on the Physics of Strongly Correlated Systems XIV: Fourteenth Training Course in the Physics of Strongly Correlated Systems, 5–16 October 2009, Vietri sul Mare, Italy*, edited by A. Avella and F. Mancini, AIP Conf. Proc. No. 1297 (AIP, New York, 2010), pp. 135–338.
- [72] B. N. Parlett and D. S. Scott, The Lanczos algorithm with selective orthogonalization, *Math. Comput.* **33**, 217 (1979).
- [73] G. Kresse and J. Furthmüller, Efficient iterative schemes for *ab initio* total-energy calculations using a plane-wave basis set, *Phys. Rev. B* **54**, 11169 (1996).